

Initial Development of Tropical Precipitation Patterns in Response to a Local Warm SST Area: An Aqua-Planet Ensemble Study

Kensuke NAKAJIMA

Faculty of Sciences, Kyushu University, Fukuoka, Japan

Eizi TOYODA

Numerical Prediction Division, Japan Meteorological Agency, Tokyo, Japan

Masaki ISHIWATARI

Graduate School of Environmental Earth Science, Hokkaido University, Sapporo, Japan

Shin-ichi TAKEHIRO

Institute of Mathematical Sciences, Kyoto University, Kyoto, Japan

and

Yoshi-Yuki HAYASHI

Graduate School of Science, Hokkaido University, Sapporo, Japan

(Manuscript received 17 September 2002, in final form 13 July 2004)

Abstract

For the purpose of examining the initial development of the atmospheric response to a warm SST anomaly placed at the equator, an ensemble switch-on experiment is conducted with an aqua-planet GCM. An ensemble average of the size of 128 significantly reduces the transient noises caused by both small scale convective activity and large scale intraseasonal variability.

In the first three days after the switch-on of the SST anomaly, a convection center develops above the warm SST area. As a barotropic response to the heating of convection center, a global increase of surface pressure occurs outside the low pressure region around the warm SST area. The response after the emergence of the high pressure anomaly is consistent with Gill (1980); a warm Kelvin wave-like anomaly is emitted to the east of the convection center, while a warm Rossby wave-like anomaly is emitted to the west.

The Kelvin wave-like signal propagates at a speed slower than that of free Kelvin wave expected from its vertical wavelength, suggesting that the signal is a “moist” Kelvin wave. Transient decrease of precipitation occurs at the moist Kelvin wave front; a decrease of convection associated with the downward motion at the wave front is consistent with its slow propagation. After several days, precipitation recovers and is even intensified because of the surface frictional convergence associated with the Kelvin

Corresponding author: Kensuke Nakajima, 6-10-1
Hakozaki Higashi-ku Fukuoka 812-8581 Japan.
E-mail: kensuke@geo.kyushu-u.ac.jp
© 2004, Meteorological Society of Japan

wave-like equatorial low pressure anomaly. To the west of the warm SST area, on the other hand, precipitation decreases monotonically. The continuous reduction of precipitation is caused by the equatorial surface frictional divergence associated with the relatively high pressure anomaly at the equator of the Rossby wave structure.

Finally, there appears a slow zonally symmetric response within the Hadley cell characterized with surface pressure rise in the tropics and westerly wind anomaly in the troposphere. The change of eddy zonal momentum transport, together with the transport toward the lower level by the Hadley circulation and the geostrophic adjustment to the resulting low level westerly acceleration, seems to be responsible for the response.

1. Introduction

Large scale inhomogeneity of surface boundary conditions such as land-sea contrast and SST distribution plays an important role in determining the large scale distributions of precipitation and atmospheric circulation fields. However, the relationship between the inhomogeneities of the boundary conditions and the observed precipitation or circulation patterns is not straight forward. This is because the amount of precipitation is affected not only directly by the in situ surface boundary conditions but also remotely by the circulations driven by the distant features (thermal and/or topographic forcing).

With this issue in mind, Hosaka et al. (1998, hereafter, referred to as H98) investigated possible precipitation patterns over the entire tropical region with a simple "aqua-planet" setup. The surface boundary condition utilized in H98 is that only one localized warm SST anomaly is placed at the equator on a zonally and equatorially symmetric basic SST distribution. An active convection center forms over the warm SST anomaly region. By eliminating the effect of longitudinal variation of in situ surface boundary conditions, idealistic remote effects of the active convection center on the distribution of precipitation over the entire tropical region can be clarified.

The statistically steady response obtained by H98 is characterized with the east-west asymmetries of precipitation and surface pressure anomalies in the equatorial region. In an extensive region to the east of the warm SST area, precipitation is enhanced and pressure anomaly is negative. On the other hand, drying occurs and pressure rises to the west. The appearance of the high pressure anomaly to the west is particularly curious, since, according to the simple linear longwave theory of Gill

(1980), or Heckley and Gill (1984), surface pressure anomaly should be negative both to the east and to the west of the convection center (heat source).

H98 presents a possible scenario for the appearance of the east-west asymmetries of the precipitation and pressure responses as follows. In the equatorial region to the east of the warm SST area, pressure anomaly becomes negative because of the equatorial Kelvin wave response forced by the convection center. Moisture convergence toward the equator from the off-equatorial region is enhanced because of the Ekman transport in the surface boundary layer. The increase of moisture convergence leads to a precipitation increase and enhances the low pressure there to cause further intensification of the moisture convergence. At the equatorial region to the west of the warm SST area, the initial pressure anomaly should also be negative. However, the pressure anomaly at the equator is less intense than those in the off-equatorial regions because of the meridional structure of the equatorial Rossby wave response. Moisture convergence toward the equator from the off-equatorial area is weakened, since the Ekman transport in the surface boundary layer is oriented to the off-equatorial low pressure maxima. The decrease of equatorial moisture convergence causes precipitation decrease at the equator to the west of the warm SST anomaly. Because of the radiative cooling, the decrease of precipitation induces high pressure anomaly and causes further intensification of the negative anomaly of moisture convergence.

Unfortunately, it is difficult to recognize how the final steady balanced state is established from the time mean circulation field, which is the only information H98 presents. In the region to the east of the warm SST anomaly, it may be fair to admit the scenario, since the

obtained statistically steady state suggests that the surface moisture convergence associated with the equatorial low pressure anomaly intensifies the amount of precipitation. In the region to the west of the warm SST anomaly, however, there remains no clue to possible transient low pressure Rossby wave-like response; there is only the resultant high pressure anomaly and precipitation decrease.

For the purpose of verifying the scenario presented by H98, an initial switch-on experiment must be useful. Observation of the development of precipitation and circulation fields after the introduction of the SST anomaly will provide necessary information. The anticipated initial emergence of low pressure anomaly on the western side and its transition to high pressure anomaly may be directly observed. However, as is briefly discussed in H98, the initial development of the response is severely contaminated by two types of noise. One is the grid point moist convection event. The precipitation intensity associated with grid scale convection is by an order of magnitude larger than the magnitude of time-mean precipitation anomaly over the convection center above the warm SST area, which is much stronger than the remote response that is of the present interest. As a result, the response to the introduction of the warm SST anomaly can hardly be recognized in the instantaneous values. The other type of noise is eastward propagating, moist Kelvin wave, close to the temporal and spatial scales of Madden-Julian Oscillation (MJO; Madden and Julian 1972). The amplitude of the moist Kelvin wave is comparable to, or larger than, that of the response to the warm SST anomaly, so that the structure of the initial development shall be severely distorted by the signal of MJO (hereafter, the moist Kelvin wave with the longitudinal scale of wavenumber one obtained in the aqua-planet experiments is referred to as MJO).

H98 suggests that the ensemble averaging of a set of runs starting from different initial conditions may be useful in extracting the evolution of the response masked by those noises. Following this suggestion, Toyoda et al. (1999) conducted a preliminary ensemble experiment with the experimental set-up being the same as that of H98. They examined the efficiency of ensemble averaging in noise reduction by in-

creasing the size of the ensemble set up to 200, and concluded that the evolution of large scale circulation features can be satisfactory extracted by averaging 64 runs, and the precipitation feature can be recognized by averaging 128, or larger number of runs. Toyoda et al. (1999) also presented the evolution of the ensemble average profiles of surface pressure and precipitation anomaly along the equator. These figures clearly show the propagation of the pressure and precipitation signals to the east of the warm SST area with Kelvin wave-like characteristics. However, the possible existence of Rossby wave-like response is not confirmed, because off-equatorial structure of the response is not presented.

In the present paper, we extend the ensemble experiment of Toyoda et al. (1999) and try to clarify the initial development of the response field after the switch-on of the warm SST anomaly. In particular, we try to verify the scenario proposed by H98 for the evolution of the east-west asymmetry caused by the convection center over the warm SST area. The details of the time-dependent response will also be presented. These information on the temporal evolution will be useful particularly when the practical application is concerned, since the real SST distribution often varies with the time scale that is not much longer than that of the adjustment to the steady state response.

The paper is organized as follows. Section 2 describes the design of ensemble experiment. Section 3 examines the efficiency of the ensemble averaging to extract the time-dependent response caused by the SST anomaly. In Section 4, the time development of the response field is presented. In Section 5 and Section 6, the mechanism of the east-west asymmetric precipitation response, and that of slow zonally symmetric response are examined, respectively. Section 7 is devoted to discussions and conclusions.

2. Experimental design

The model used here is the same three-dimensional primitive system on a sphere as that used by H98, i.e., AGCM5 of the GFD-DENNOU CLUB edition (Swamp Project 1998). The physical and dynamical processes of the model are summarized as follows (as for the

details, see Numaguti 1992, or Hayashi et al. 2000). The dynamical part is represented by the pseudo spectral method with the triangular truncation at wavenumber 42 (T42) and by the sigma vertical coordinate with 16 vertical levels. The moist processes are represented by the large scale condensation and the moist convective adjustment (Manabe et al. 1965). Condensed water is removed from the system immediately after condensation; there are no clouds. The radiation model includes only the absorption and emission of longwave; scattering of longwave radiation is not included. The longwave absorption coefficients are empirically chosen so that the cooling profile of the atmosphere roughly resembles the observed one. The vertical turbulent mixing is represented by the level 2 scheme of Mellor and Yamada (1974). The surface fluxes of momentum, heat and water vapor are evaluated by the bulk formula (Louis 1979).

The ensemble experiment consists of 128 GCM runs. Each run is integrated for 50 days, starting from a different initial condition with the common SST distribution shown in Fig. 1. The integration period, 50 days, is presumably long enough for the tropical precipitation response to be completed; according to the experience of H98 and Toyoda et al. (1999), establishment of the western dry region can be recognized in about 20 days, although it is quite hard to recognize the dry area in Fig. 6 of H98 since it is so noisy. The SST distribution, which is the same as that for case A4 of H98, consists of a patch of localized warm SST anomaly superimposed on the equatorially symmetric, zonally uniform basic SST distribution. The local warm SST area is rectangular shape with a longitudinal extent of 40° and a latitudinal extent of 20° , and its center is placed at the equator. The peak value of

the SST anomaly is 4 K; the actual maximum value achieved at the grid point is 3.4 K. For the sake of comparison between the ensemble and temporal averages, a separate, long-term integration with the SST anomaly is performed. The time series between 700 days and 2100 days is used to calculate the temporal averaging.¹

The initial conditions of the ensemble runs are sampled in the same way as Toyoda et al. (1999) from the time series of an experiment without SST anomaly. The sampling is performed every 50 days from the 700th day to the 7100th day of the integration period. Spectral analysis of the tropical precipitation field in the experiment without SST anomaly shows that the MJO period is about 36 days (not shown here, but a result of the similar experiment can be seen in Fig. 8 of Hayashi et al., 2000). Since the sampling period of 50 days and the MJO period of 36 days do not have a small common multiple, the MJO signal is expected to be considerably reduced after the ensemble mean operation. We also assume that the sampling interval of 50 days is long enough to reduce the coherency of the small scale noise. The long-term integration without SST anomaly is also used as the reference to which the results of the experiments with SST anomaly are compared. The temporal and zonal mean meridional cross sections of temperature, zonal wind, mass stream function, and meridional distribution of surface precipitation of the run without SST anomaly are shown in Fig. 2.

Toyoda et al. (1999) defines the ensemble mean anomaly as the difference between the ensemble averaged field obtained from the runs with SST anomaly and the zonally, temporally averaged field of the run without SST anomaly. As is quoted in Section 1, the number of samples in the present study, 128, is large enough

1 We have to mention that, if we carefully compare the equatorial precipitation anomaly in the long term run obtained in the present study and that of case A4 of H98, the former is a bit weaker than the latter, although the experimental setups are basically the same. There appears to be significant difference between the zonal mean field of the experiment without SST anomaly in H98 and that in the present study; for example, the precipitation peak of ITCZ at the equator in H98 is sharp, whereas that in the present study is broad. Difference is also recognized in the long

term mean surface pressure anomaly field, where the area of equatorial negative anomaly shrinks (Fig. 4 (c)) compared to H98. The reason why the difference is caused has not been clearly understood. It may originate from the machine implementation of the model equations or the slight difference of binary representation of the basic state SST distribution. The model performance under the aqua planet condition with the similar setup used here is summarized in Hayashi et al. (2000).

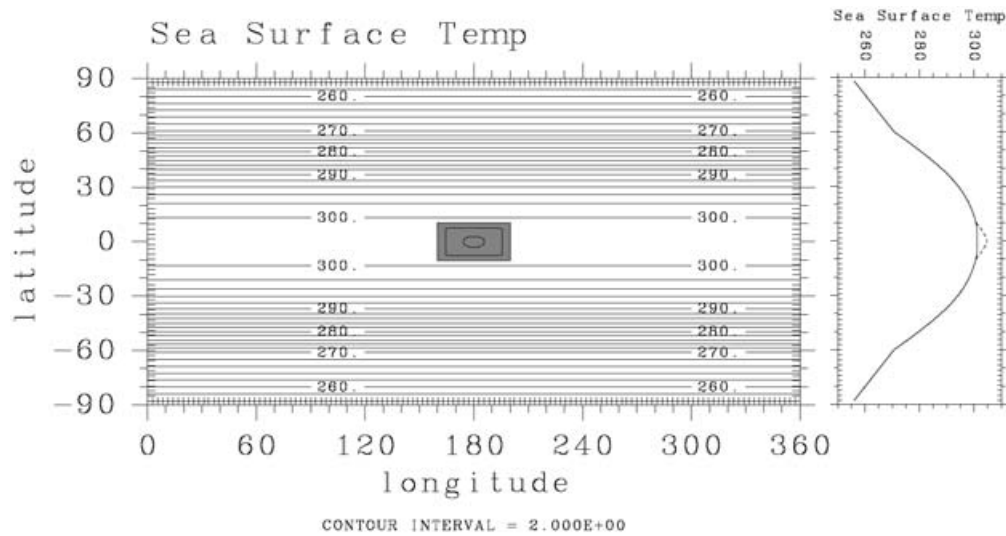


Fig. 1. Distribution of SST utilized in the experiment. Left panel shows the horizontal distribution. Local warm SST area is shaded. Right panel shows the latitudinal profiles of basic SST distribution (solid line) and SST anomaly (dashed line) at the longitude 180° where the magnitude of anomalous SST is the maximum. Unit is K.

to examine the large scale features of the tropical response to the SST anomaly. However, there remain two kinds of noise originating from grid scale convection in the tropics and baroclinic waves in the extratropics, which obscure detail of the response seen as ensemble mean anomaly defined above.

In this paper, in addition to the definition of ensemble mean anomaly of Toyoda et al. (1999), we will use another definition of ensemble mean anomaly which is calculated as follows. Because of the way we prepared the set of initial conditions for the ensemble experiment, each of the 50 day SST anomaly runs has a 50 day time series of the SST anomaly-free run that starts from the same initial condition as that of the SST anomaly run. We can define an anomaly of a field for each SST anomaly run as its departure from that for the corresponding SST anomaly-free time series. The ensemble mean anomaly is then defined as the ensemble average of thus calculated anomalies. Hereafter, when we need to distinguish those two definitions of ensemble mean anomaly, the definition by Toyoda et al. (1999) is referred to as “ensemble mean anomaly from zonal and temporal average”, while that defined here is referred to as “ensemble mean anomaly from individual”.

The advantage-disadvantage of the two definitions of the ensemble mean anomalies depends on the integration period from the initial switch-on. In the first several days, ensemble mean anomaly from individual proves to be more efficient in extracting the response to the introduction of the SST anomaly; the coherence of the transient noises in each pair of SST-anomaly run and SST-anomaly-free run starting from the same initial condition remains high for some initial duration (the precise time duration depends on the variable concerned). After this initial period, ensemble mean anomaly from zonal and temporal average becomes more efficient in extracting the mean response. This is because the coherence between the transient noises in each pair of SST-anomaly run and SST-anomaly-free run is lost; the transient noises in both runs contribute to the total noise amplitude of ensemble mean anomaly from individual.

As far as the large scale features in the tropics are concerned, both of the two definitions of the ensemble mean anomalies are expected to extract the same information as we increase the ensemble size. In the following sections, we select one of the two definitions case by case by consulting which of the two gives the smoother field of the variable concerned.

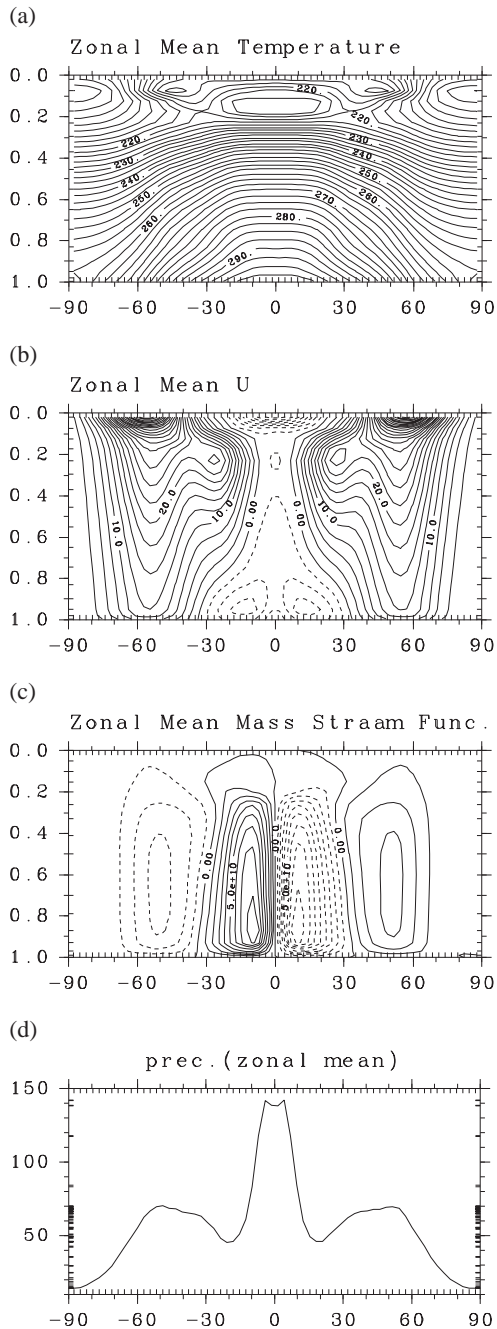


Fig. 2. Zonal and temporal mean fields of the experiment without SST anomaly; (a) temperature (contour interval is 2.5 K), (b) zonal wind (contour interval is 2.5 m s^{-1}), (c) meridional mass stream function (contour interval is $10^{10} \text{ Kg m}^{-1}$), and (d) precipitation (w m^{-2}). 12 hourly data from day 700th to 7100th are used for time averaging.

3. Effectiveness of ensemble averaging in noise reduction

Before examining the time evolution of the atmospheric response to the introduction of the warm SST area, we briefly demonstrate the effectiveness of the ensemble experiment. For that purpose, we compare precipitation and pressure fields in the long-term average and those in the ensemble average at $t = 50$ day. By this time, as will be shown in Section 4, the rainfall response in the tropics settles down to the structure of the steady state response, including its east-west asymmetry.

Figures 3 (a) and (b) show the horizontal distributions of the precipitation anomaly from zonal and temporal average at day 50 obtained by a single run, and that by the average of 128 runs, respectively. The response obtained by a single run (Fig. 3 (a)) is characterized with a number of positive anomalies and zonally distributed negative anomalies. The positive anomalies correspond to moist convection activities associated with various transient disturbances, although the coarse resolution of the present model does not permit precise representation of their structure. Midlatitude anomalies are associated with baroclinic waves, and those in the tropics can be regarded as super clusters along the equator and tropical cyclones along the ITCZs, as is reported in Numaguti and Hayashi (1991). The zonally distributed negative anomalies are the reflections of the long-time mean precipitation zones, i.e., ITCZs and mid-latitude baroclinic zones. In all latitudinal bands, positive anomalies are so intense that the signatures caused by the SST anomaly, including the convection center itself whose peak value is about 500 W m^{-2} , can be hardly recognized.

In the response obtained by the 128 ensemble average (Fig. 3 (b)), the convection center appears quite prominently as the positive anomaly above the warm SST area. To the east of the convection center, positive precipitation anomaly prevails along the equator, while, to the west of the convection center, negative anomaly is evident. North-south symmetric mid-latitudes anomalies, the most notable of which are located around $(\pm 30^\circ \text{N}, 200^\circ \text{E})$, can also be recognized. These are presumably associated with the stationary planetary wave

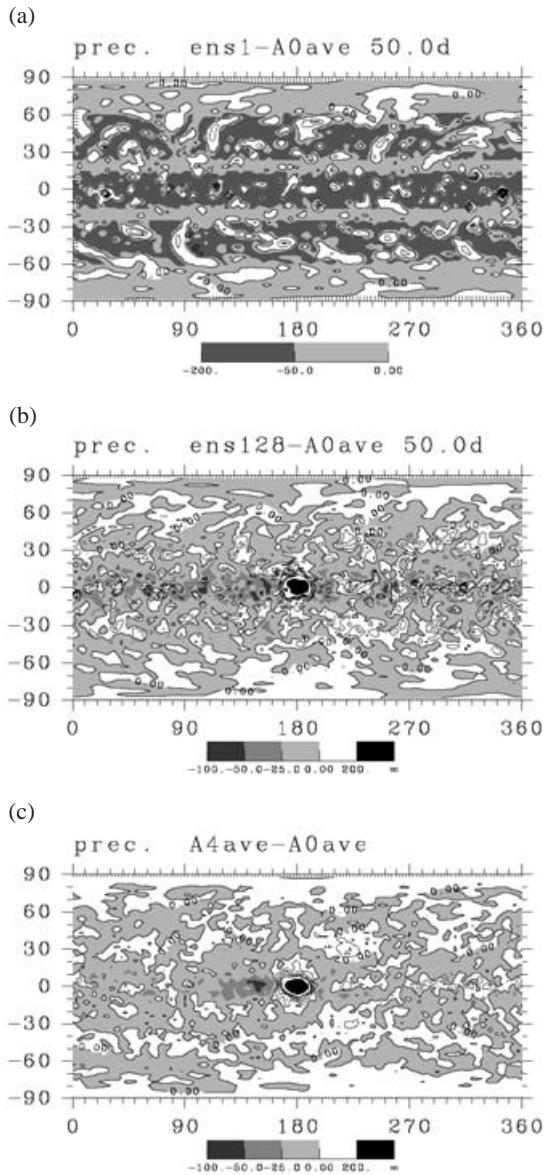


Fig. 3. Horizontal distributions of precipitation anomaly from zonal and temporal average; (a) at day 50 of 1 run, (b) at day 50 of 128 run mean, and (c) time mean of the long term anomaly experiment. Unit is $W m^{-2}$. Contour interval is $500 W m^{-2}$ for (a), and is $20 W m^{-2}$ for (b) and (c).

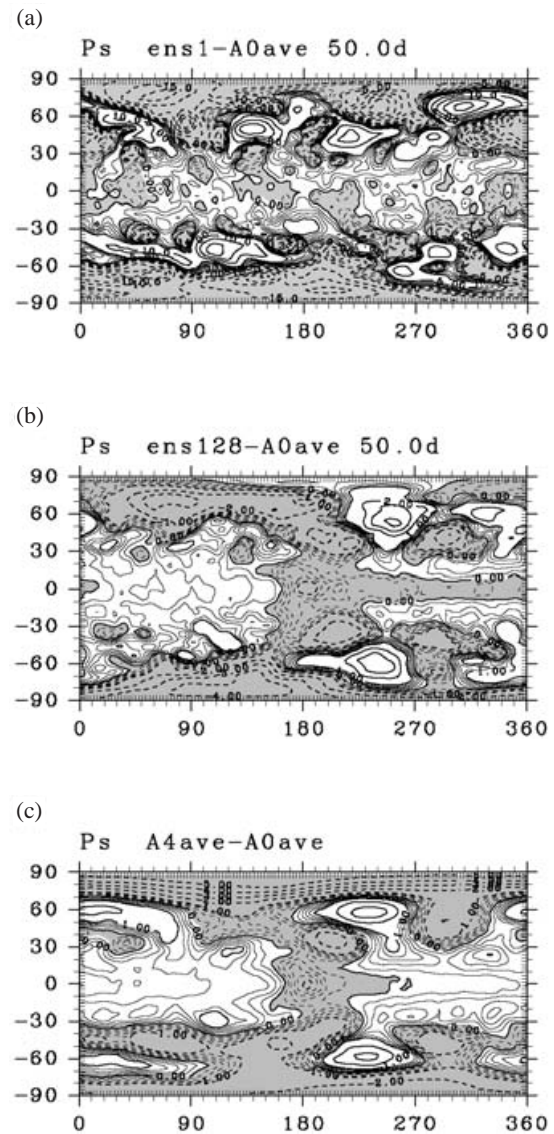


Fig. 4. Horizontal distributions of surface pressure anomaly (p') from zonal and temporal average: (a) At day 50 of 1 run. Contour intervals are 1 hPa and 5 hPa for $|p'| < 5$ hPa and $|p'| > 5$ hPa, respectively. Regions with negative p' are shaded. (b) At day 50 of 128 run mean. Contour intervals are 0.2 hPa and 1 hPa for $|p'| < 1$ hPa and $|p'| > 1$ hPa, respectively. Regions with negative p' are shaded. (c) Same as (b) but for time mean of the long term anomaly experiment.

packets emitted from the convection center (see Fig. 4 (b)). Compared to the time mean anomaly field (Fig. 3 (c)), the ensemble mean anomaly field (Fig. 3 (b)) is more noisy. The noise is more intense in the tropics than the other latitudes and has a small scale, which indicates that its main origin is grid scale convective events in the tropics. However, as a whole, it can be concluded that the large-scale pattern shown in the ensemble mean anomaly, including its east-west asymmetry in the tropics, reproduces that of the long time-mean response fairly well.

Figures 4 (a) and (b) show the horizontal distributions of the surface pressure anomalies from zonal and temporal average at day 50 obtained by a single run and that by the average of 128 runs, respectively. In the result of the single run (Fig. 4 (a)), little signature of the warm water-related features can be found as in the case of precipitation. In the 128 ensemble mean anomaly field (Fig. 4 (b)), low pressure area over the warm SST area is quite evident. We can clearly observe an east-west asymmetric pressure response along the equator and wavetrains propagating to the mid-latitudes.

Comparing the 128 ensemble mean anomaly field (Fig. 4 (b)) with the time mean anomaly field (Fig. 4 (c)), we can notice a few differences. Firstly, especially in higher latitudes, the locations of individual peaks of high or low anomalies differ between the ensemble and the long time mean anomaly fields. Secondly, pressure in the tropics is generally lower in the ensemble average than in the long time mean. Thirdly, significant negative anomalies at the poles in the long time mean, whose north-south asymmetry will be touched shortly, are absent in the ensemble average.

There are two possible causes for these discrepancies.² The first concern, which naturally occurs in one's mind, is that the integration duration of the ensemble run, 50 days, is not long enough for the establishment of the global steady response. The effects of the shortness of

the integration period on the zonal mean tropical response will be discussed in the following sections. The second concern is the intrinsically high "noise level" of the pressure in the higher latitudes. As can be observed in Fig. 4 (a), the instantaneous amplitude of pressure perturbation in the middle and high latitudes exceed 10 hPa. Assuming that pressure signals of those mid- and high latitude disturbances are random in the 128 members of the ensemble experiment, the amplitude of the resultant noise in the ensemble average shall be reduced to $1/\sqrt{128}$ of the original amplitude, i.e., about 1 hPa. On the other hand, consulting Fig. 4 (c), the typical amplitude of the mid- and high latitude pressure anomalies forced by the SST anomaly is about 3 hPa. Consequently, a "perfect" reproduction of the time-mean signal by the ensemble average of the size of only 128 members is hard to be expected.

Another problem in the higher latitudes is the existence of very long-timescale variability. Temporal spectrums of the extratropical pressure variation at high latitudes (not shown here) are fairly red for both the long-term run with SST anomaly and the long-term run without SST anomaly; characteristic amplitudes of the high latitude zonal mean pressure variation with the period of about 1000 days roughly reach 10 hPa. In order to smooth out those noises due to the slow variabilities, the periods of the runs (1400 days for SST anomaly free case and 2200 days for SST anomaly case) are not long enough. It is also anticipated that the initial conditions for the ensemble experiment sampled from the period of 6400 day are not distributed very uniformly over the phase of the slow extratropical variabilities, since the period can not be regarded as long enough compared to the time scale of the long-term variabilities. Considering these issues, the details of the response in the higher latitudes can be examined only by comparing an ensemble average of the still larger number of samples with a temporal average over the still longer time period. Sampling of the initial conditions from still longer time series of SST anomaly free run will also be required.

Summarizing this section, we can conclude that the notable features of the time-mean response in the tropics to the existence of the warm SST anomaly, i.e., the east-west asym-

² Logically, there is the third concern, which is more fundamental; the ergodicity of the response. However, we are not going to step into this deep issue. We are assuming that the response is ergodic.

metry of the precipitation and pressure anomalies, are captured fairly well by the 128 run ensemble mean response at day 50. We can expect that the development sequence of the atmo-

spheric response is captured in the time series of the ensemble mean anomaly. In the following sections, the results obtained by the ensemble set with the size of 128 are presented.

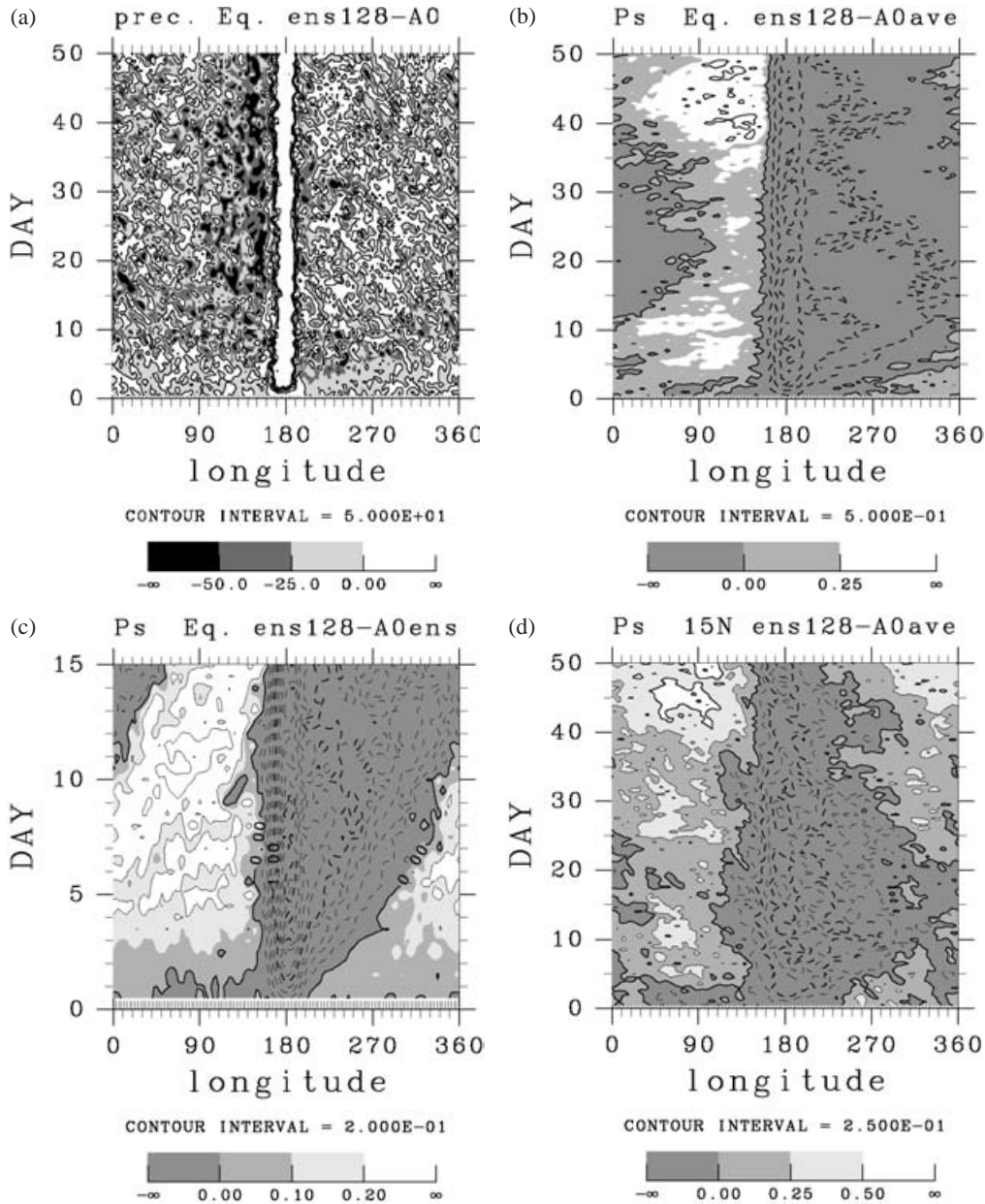


Fig. 5. Time-longitudinal cross sections of ensemble mean anomalies; (a) precipitation ($W m^{-2}$) at the equator (the ensemble mean anomaly from individual is plotted before $t = 10$ day), (b) surface pressure (hPa) at the equator, (c) same as (b) but the ensemble mean anomaly from individual during the first 15 days, and (d) surface pressure (hPa) at $15^{\circ}N$. Note that (a), (b) and (d) are ensemble mean anomalies from zonal and temporal average, while (c) is ensemble mean anomaly from individual.

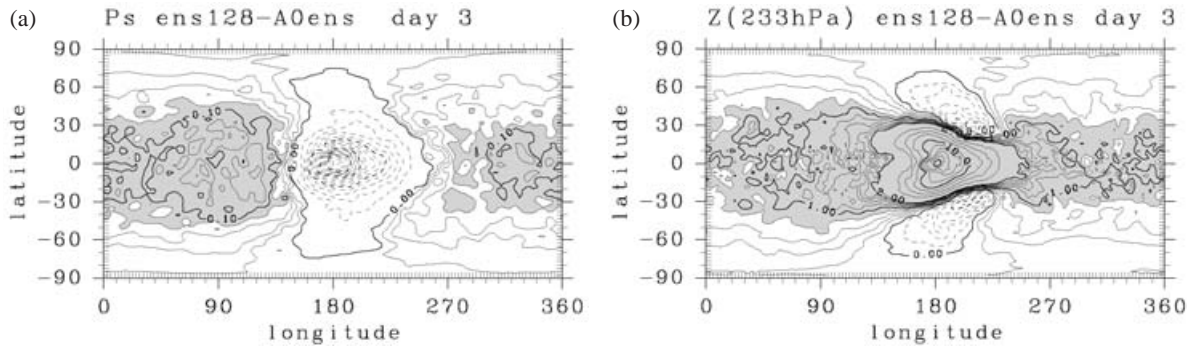


Fig. 6. Ensemble mean anomaly from individual at day 3; (a) surface pressure and (b) geopotential height at 233 hPa. Contour interval is 0.02 hPa for positive pressure anomaly, and is 0.1 hPa for negative pressure anomaly. Area with the pressure anomaly larger than 0.08 hPa is shaded. Contour interval is 0.2 m for geopotential anomaly smaller than 2 m, and is 2 m for the larger anomaly. Area with geopotential anomaly larger than 0.8 m is shaded.

4. Development of the response

Figure 5 (a) and Figure 5 (b) show the time evolutions of the ensemble mean anomalies from zonal, temporal average of precipitation and pressure along the equator, respectively. The response in the first three days is characterized by a rapid pressure lowering over the area of SST anomaly. This rapid pressure descend is caused by the quick rises of temperature and mixing ratio within the surface boundary layer (not shown here) driven by the sensible and latent heat fluxes from the warm SST anomaly. Increase of precipitation over the warm SST area immediately follows the pressure decrease, although it takes several days for the convection center to be fully established.

Associated with the precipitation increase at the convection center, a widespread pressure rise occurs. Figure 5 (c) shows that the pressure rise begins almost simultaneously over the wide area of the equatorial circumference in the first three days. Actually, the response is spreading globally as is exemplified in Fig. 6 (a), where the horizontal distribution of pressure anomaly at day 3 is plotted. Except for the low pressure area around the convection center and the signatures of mid latitude Rossby waves, the pressure response is positive over the globe.

Comparison between the surface pressure response (Fig. 6 (a)) and the geopotential height response in the upper troposphere (Fig. 6 (b)) suggests that the globally distributed sur-

face high pressure anomaly, as well as the low pressure anomalies in the mid latitudes to the north and south of the SST anomaly, has a barotropic vertical structure. Geopotential perturbation of a Lamb wave is vertically one signed and is approximately proportional to $T/T_s \exp[gz/C_p T]$, which gives the value of 1.14 for the ratio of geopotential perturbation at 233 hPa to that at the ground surface. Considering that 0.1 hPa of surface pressure anomaly corresponds to about 0.86 m of geopotential height anomaly at the surface, the perturbation magnitudes shown in Fig. 6 (a) and Fig. 6 (b) prove that the globally spreading positive response, outside the area at and around the SST anomaly, is explained as a Lamb wave.³ Actually, the evolution in the first day of the ensemble mean field (not shown here) clearly shows its expansion from the area of SST anomaly at the speed of sound wave. The moderate confinement of the barotropic response to the lower latitudes is understood by the equatorial radius of deformation for the sound velocity, $(c_s/\beta)^{1/2} = (315[\text{ms}^{-1}]/2.3 \cdot 10^{-11}[\text{s}^{-1}\text{m}^{-1}])^{1/2} = 3660[\text{km}]$.

As discussed by Nicholls and Pielke (1994),

³ Note that the hydrostatic system can correctly represent Lamb waves (e.g., Gill 1982a). Since the model is discretized, the divergent component associated with the barotropic mode of vertical mode decomposition (e.g., the “first” vertical normal mode in Kasahara and Shigehisa (1983) with the equivalent height of about 10100 m) is regarded as the Lamb wave.

barotropic response acts as the agent that redistributes mass exported from the area of pressure fall around the SST anomaly. As the divergent component of this barotropic response, a Lamb wave is excited by the heating in the convection center, which causes the rapidly spreading component of the initial surface pressure response. At $t = 10$ days, the pressure rise to the west of the SST anomaly caused by the initial barotropic response amounts to 0.25 hPa, which is by no means negligible; it is already about 40% of the amplitude of the high pressure anomaly to the west of the warm SST area observed in the steady response in Fig. 4 (c), or that obtained by H98. This suggests that a considerable portion of the pressure rise to the west of the convection center can be understood as the result of the extensive accumulation of the air expelled by heating at the convection center.

Following the development of the initial barotropic response, the east-west asymmetric feature begins to emerge. As can be observed around the convection center in Fig. 6, the east-west asymmetric feature has a warm baroclinic structure, where low pressure perturbation exists in the lower levels, while high pressure perturbation exists in the upper levels. Figure 7 shows the evolution of geopotential height response in the lower troposphere at the 841 hPa pressure level. The response to the east of the SST anomaly has a warm Kelvin wave-like structure; the low pressure anomaly has its lowest value at the equator, and is confined around the equatorial latitudes, and extends eastward. The temperature anomaly (not shown) is positive in the mid troposphere, and the zonal wind anomaly in the troposphere (not shown) is almost in a geostrophic balance with the geopotential anomaly. The speed of the eastward extension of the warm Kelvin wave like response is around 18 m s^{-1} , which is significantly slower than the horizontal phase velocity of dry Kelvin wave of the same vertical wavelength, which is about 40 m s^{-1} .⁴

This slowness implies that the eastern front of the response can be regarded as a “moist”

4 For example, in Kasahara and Shigehisa (1983), the equivalent height is about 180 m (corresponding wave speed is 42 m s^{-1}) for their “fourth” vertical normal mode that has only one node (near $\sigma = 0.5$) in the troposphere.

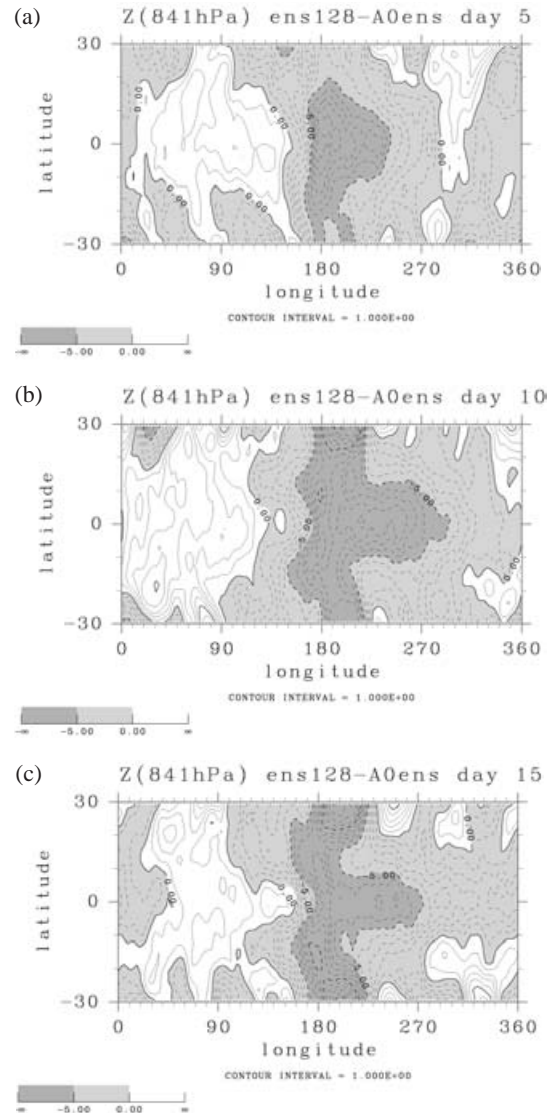


Fig. 7. Response of geopotential height at 841 hPa pressure level at (a) 5 day, (b) 10 day, and (c) 15 day. Contour interval is 1 m.

Kelvin wave. In Fig. 5 (a), it can be recognized that precipitation is suppressed at around the propagating front. Since downward flow exists at the wave front (not shown), this implies that latent heat release is positively correlated with vertical velocity. The resulting reduced stability effect (Gill 1982b) explains the slowness of the eastward extension of the response.

The subsequent development, however, deviates from that expected from the moist Kelvin

structure; precipitation anomaly begins to rebound and becomes positive in a few days after the passage of the response front. The mechanism of the increase of precipitation will be examined later. With this change of the signature of the precipitation anomaly, the structure of response to the east of the SST anomaly approaches that of H98, which is characterized by a zone of negative pressure and positive precipitation anomaly, extending eastward along the equator from the convection center.

To the west of the SST anomaly, the response in the first several days has a warm Rossby wave characteristics. Pressure perturbation along the latitude of 15° is negative, while there appears little pressure signal along the equator (Fig. 7). The western front of the pressure response is somewhat obscure compared to the eastern moist Kelvin front. Recalling that a Rossby response emitted by a narrow heat source is longitudinally dispersive, it is reasonable that the western response front is not as sharp as the eastern front. The pressure response propagates westward at the speed of around 6 m s^{-1} , according to the extension of the zero pressure anomaly line of the first 10 days in Fig. 5 (d) or Fig. 7. The beginning of the precipitation decrease, associated with the western front, is also obscure compared to that at the eastern front. But a significant precipitation decrease does start as the passage of the Rossby wave front and seems to result in a reduced gravity effect. In this crude sense, we may say that the front of the western response is a "moist" Rossby wave, as is the case with the eastern response front. If the reduced gravity effect operates on the Kelvin and Rossby wave fronts with the same magnitude, the ratio of their propagation speeds remains about 1:3, which is the ratio of phase speeds between 1st Rossby wave and Kelvin wave predicted by the equatorial wave theory with long wave approximation (e.g., Matsuno 1966; Gill 1980). This is roughly true in the present case; the Kelvin and Rossby wave fronts propagate at about 18 m s^{-1} and 6 m s^{-1} , respectively. The noteworthy point in the precipitation response to the west of the SST anomaly, is that it continues to decrease even after the passage of the front. This contrasts to the behavior of precipitation to the east of the SST anomaly, where precipitation rebound occurs after the passage.

The mechanism of the continuous decrease of precipitation will be examined later.

Our result shows that the eastward propagation of the moist Kelvin wave front is actually very coherent and long lasting (Fig. 5 (b)); the moist Kelvin front can be traced encircling the equatorial circumference. The westward propagation of the moist Rossby wave front, on the other hand, is considerably blurred and, moreover, pauses around day 15. In Fig. 5 (a) and Fig. 5 (d), it seems that the moist Rossby wave extension stops simultaneously with the development of the negative precipitation anomaly to the west of the warm SST area.

It is at around day 15 that the precipitation response over the entire tropics develops into the east-west asymmetric distribution; precipitation decrease to the west, and increase to the east along the equator. The east-west pressure difference across the convection center also establishes at around day 15; pressure increase to the west, and decrease to the east along the equator. However, the absolute value of pressure response continues to change, since the zonally symmetric components of the response are still under development. Figure 8 (a) shows time evolution of the zonally averaged surface pressure response. The amount of the pressure rise in the tropics in the latter half of the integration period reaches about 0.35 hPa. Furthermore, Fig. 8 (a) suggests that the slow evolution of zonally averaged surface pressure has not completed at the end of the integration time (50 days). The existence of the remaining pressure rise can be also inferred from the difference between the ensemble mean pressure anomaly at day 50 (Fig. 4 (b)) and the time mean pressure anomaly (Fig. 4 (c)); in the tropics, the latter is almost uniformly higher than the former by about 0.25 hPa.

In contrast with the pressure response (Fig. 8 (a)), the temperature response in the mid-troposphere (Fig. 8 (b)) exhibits little change after the establishment of the east-west asymmetric response ($t \sim 20$ day). This is also true for the temperature response in whole of the troposphere. On the other hand, gradual westerly acceleration of zonal wind occurs. The westerly anomaly appears at the equatorial area in the upper troposphere (Fig. 8 (d)), and then it extends to the lower layer. The westerly anomaly in the lower layer (Fig. 8 (c)) is most

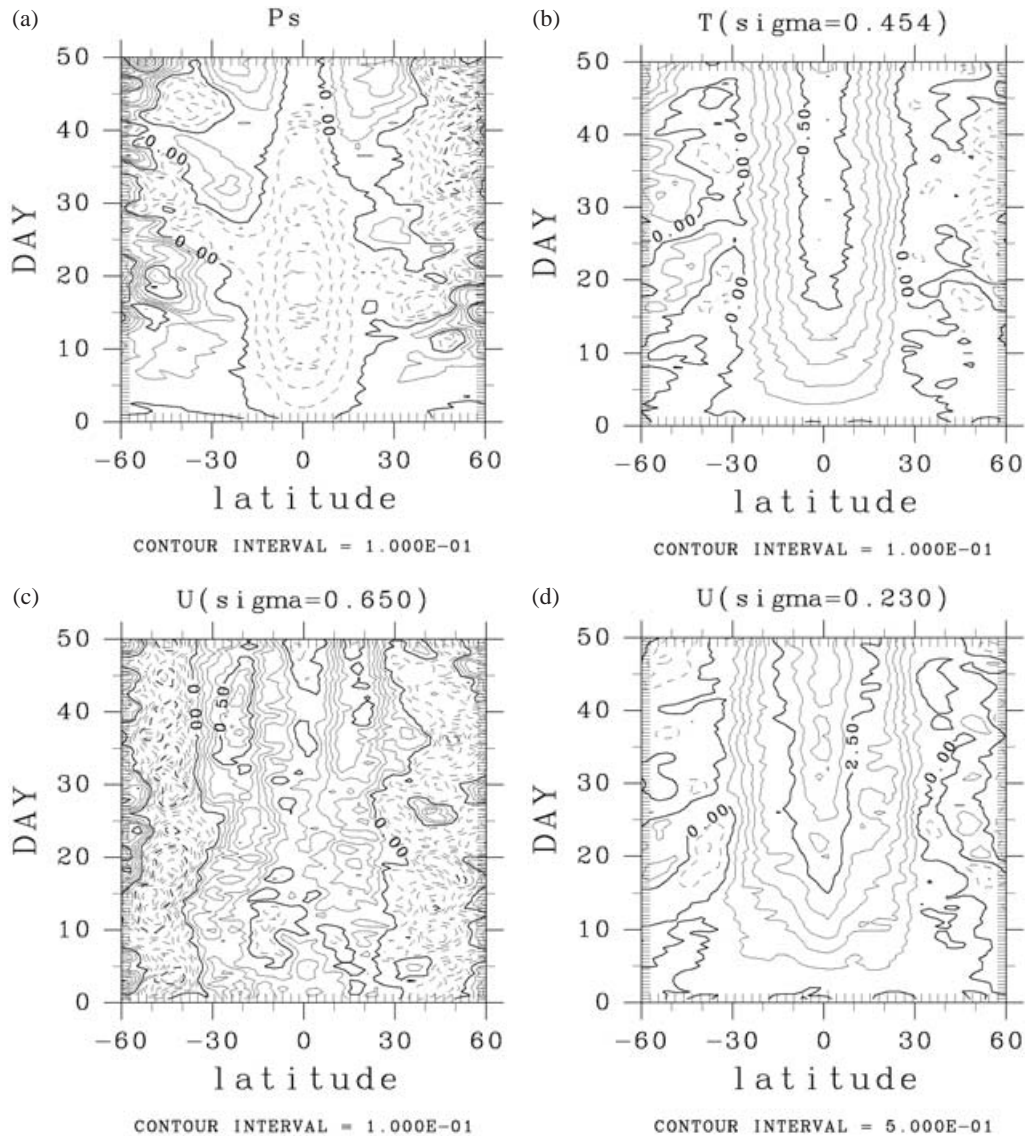


Fig. 8. Time-latitude cross sections of zonally averaged ensemble mean anomalies from individual; (a) surface pressure (hPa), (b) temperature (K) in the mid troposphere at the level of $\sigma = 0.454$, (c) westerly wind (m s^{-1}) in the lower troposphere at the level of $\sigma = 0.650$, and (d) westerly wind (m s^{-1}) in the upper troposphere at the level of $\sigma = 0.230$.

significant in the downward branch of the Hadley cell. The nature of the slow tropical pressure rise will be examined in Section 6.

5. Causes of the east-west asymmetry of precipitation

Part of the development of the atmospheric response outlined in the previous section agrees with our expectation in Section 1; warm Kelvin and warm Rossby wave-like responses

develop initially. The aspects which we have not expected are the rapid initial barotropic pressure response and the long-lasting zonally symmetric pressure development. These two responses explain a considerable amount of high pressure anomaly which remains to the west of the warm SST region in the steady state response. In this section, we will examine the cause of the east-west asymmetry of precipitation anomaly in detail; it is the meri-

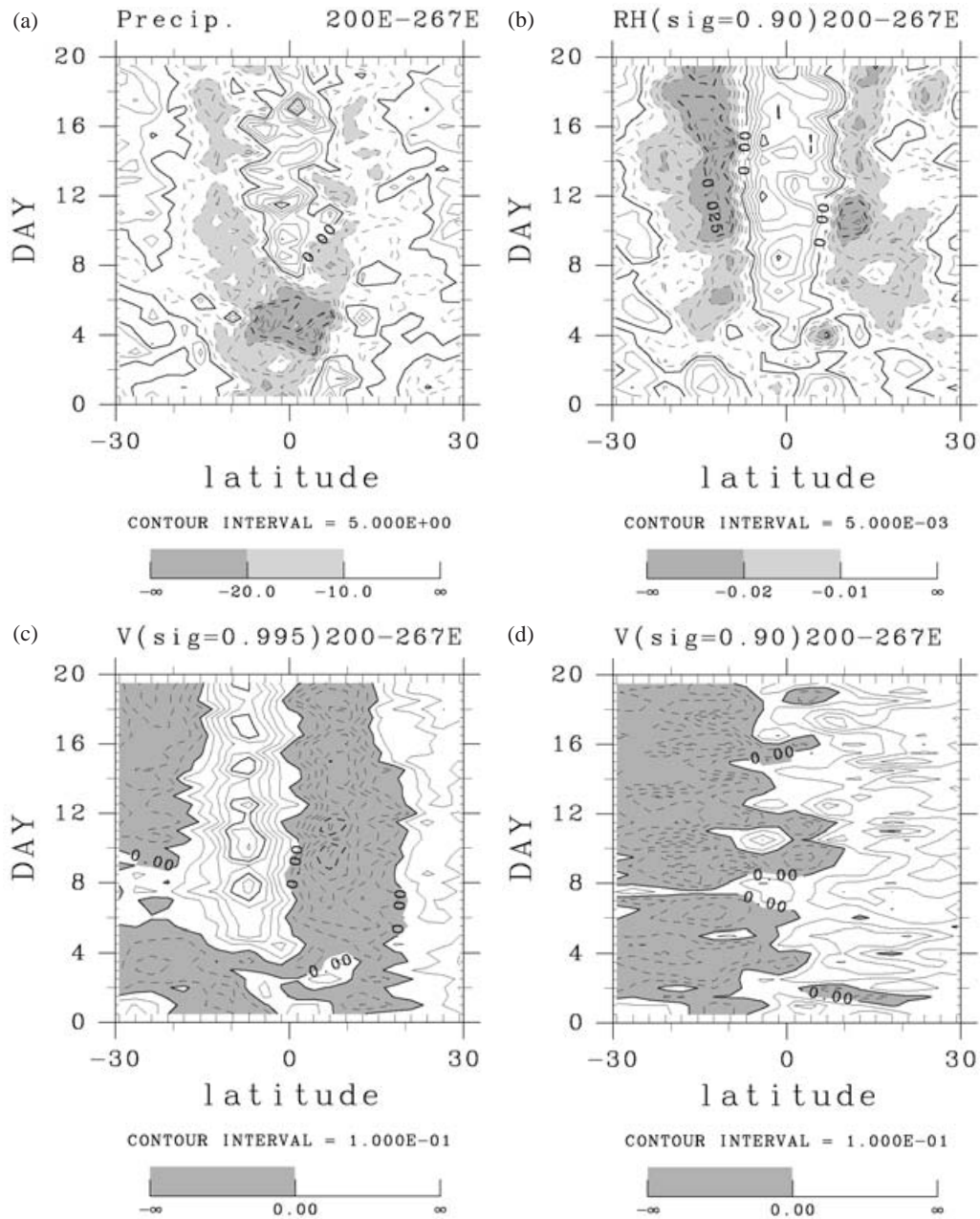


Fig. 9. Time evolution of the ensemble mean anomalies from zonal and temporal average to the east of the warm SST area during the first 20 days averaged zonally in the longitudinal region from 200° to 267°; (a) precipitation (W m^{-2}), (b) relative humidity at $\sigma = 0.9$, (c) southerly wind (m s^{-1}) at $\sigma = 0.995$, and, (d) southerly wind (m s^{-1}) at $\sigma = 0.9$.

dional convergence induced by surface friction in the planetary boundary layer.

Figure 9 shows the time evolution of the response to the east of the warm SST area averaged zonally in a longitudinal region from 200° to 267°. This is the region where the positive

precipitation anomaly develops along the equator in the steady-state response. In Fig. 9 (a), it is clearly recognized that the precipitation is suppressed at around day 5, when the Kelvin wave front arrives as mentioned in the previous section. The rebound of the precipitation

anomaly occurs at around day 8. It is noteworthy that the appearance of the equatorial positive precipitation anomaly is accompanied with the decrease of precipitation at the off-equatorial regions around the latitudes of $\pm 12^\circ$. In Fig. 9 (b), it can be seen that the relative humidity at the top of the mixed layer along the equator begins to increase at day 6, which is earlier than the recovery of precipitation by about 2 days. Furthermore, in Fig. 9 (c), the moistening along the equator can be regarded as a result of the anomalies of meridional flow in the mixed layer around the latitudes of $\pm 8^\circ$ converging toward the equator, which begins to develop just after the arrival of the Kelvin response front. As inferred from the comparison between Fig. 9 (c) and Fig. 9 (d), the meridional flow converging to the equator is vertically confined within the layer affected by surface friction. The time sequence of the development shown above proves that the increase of precipitation to the east of the warm SST area is caused by the frictional inflow toward the equator, where the pressure trough of the moist Kelvin wave develops.

Figure 10 shows the time evolution of the response to the west of the warm SST area averaged zonally in a longitudinal region from 129° to 158° . This is the region where the negative precipitation anomaly develops along the equator in the time-mean response. The arrival of the moist Rossby wave front (Fig. 7 (b)) is noted by the beginning of the meridional flow converging to the equator at around day 4. It occurs simultaneously near the ground surface (Fig. 10 (c)) and above the mixed layer (Fig. 10 (d)). This intense meridional convergence does not contribute to the increase of precipitation at the equator, since the Rossby wave front is associated also with zonal flow divergence, which exceeds the meridional convergence. Actually, precipitation decrease starts as the arrival of the Rossby wave front (Fig. 10 (a)) associated with the downdraft of the wave front. The equatorial precipitation continues to decrease, and its feature becomes clear at around day 10 (Fig. 10 (a)). At around day 10, positive precipitation anomalies also appear around the latitudes of $\pm 15^\circ$. These precipitation anomalies develop almost simultaneously with the response of relative humidity at the top of the mixed layer (Fig. 10 (b)). Relative humidity de-

creases near the equator, while it increases at the off-equatorial areas. The precipitation and humidity responses are associated with the anomalies of low level meridional flow along the latitudes of $\pm 10^\circ$ (Fig. 10 (c)), which results in the appearance of the equatorial divergence and off-equatorial convergence areas.

It can be suggested that the continuous decrease of equatorial precipitation to the west of the warm SST area results from the frictional divergence of the surface flow from the equator to the longitudes of $\pm 15^\circ$, where the pressure trough of the moist Rossby wave develops. Figure 7 (b) indicates that the Rossby wave front has passed over the area concerned here at the time of day 10. To the north and the south of the equator, the geostrophic wind above the surface mixed layer along the latitudes of about 8°N and 8°S are settled to westerly from north-westerly and south-westerly, respectively. If surface friction is considered, the low level flow further turns to off-equatorial direction, so that the equatorial region will be the area of divergence, and the continuous decrease of rainfall can be expected. In fact, as inferred from the comparison of Fig. 10 (c) and Fig. 10 (d), the meridional flow diverging from the equator is vertically confined within the layer affected by surface friction.

With respect to the signature of the anomalies of precipitation and meridional low level divergence, the responses to the east and to the west of the warm SST area contrast markedly with each other. However, they are governed by the common basic mechanism, i.e., the surface frictional flow divergence or convergence. Our expectation described in Section 1, that the surface frictional flow associated with the equatorial wave response plays a major role in the development of the precipitation response is, therefore, proved to be correct.

6. Causes of the zonally symmetric response

The slow zonally symmetric pressure rise in the tropics (Fig. 8 (a)), part of which is expected to occur after the termination of the experiment at $t = 50$ day, is an important component of the high pressure anomaly to the west of the warm SST area in the steady response. Absence of the corresponding temperature response (Fig. 8 (b)), and presence of the corresponding westerly

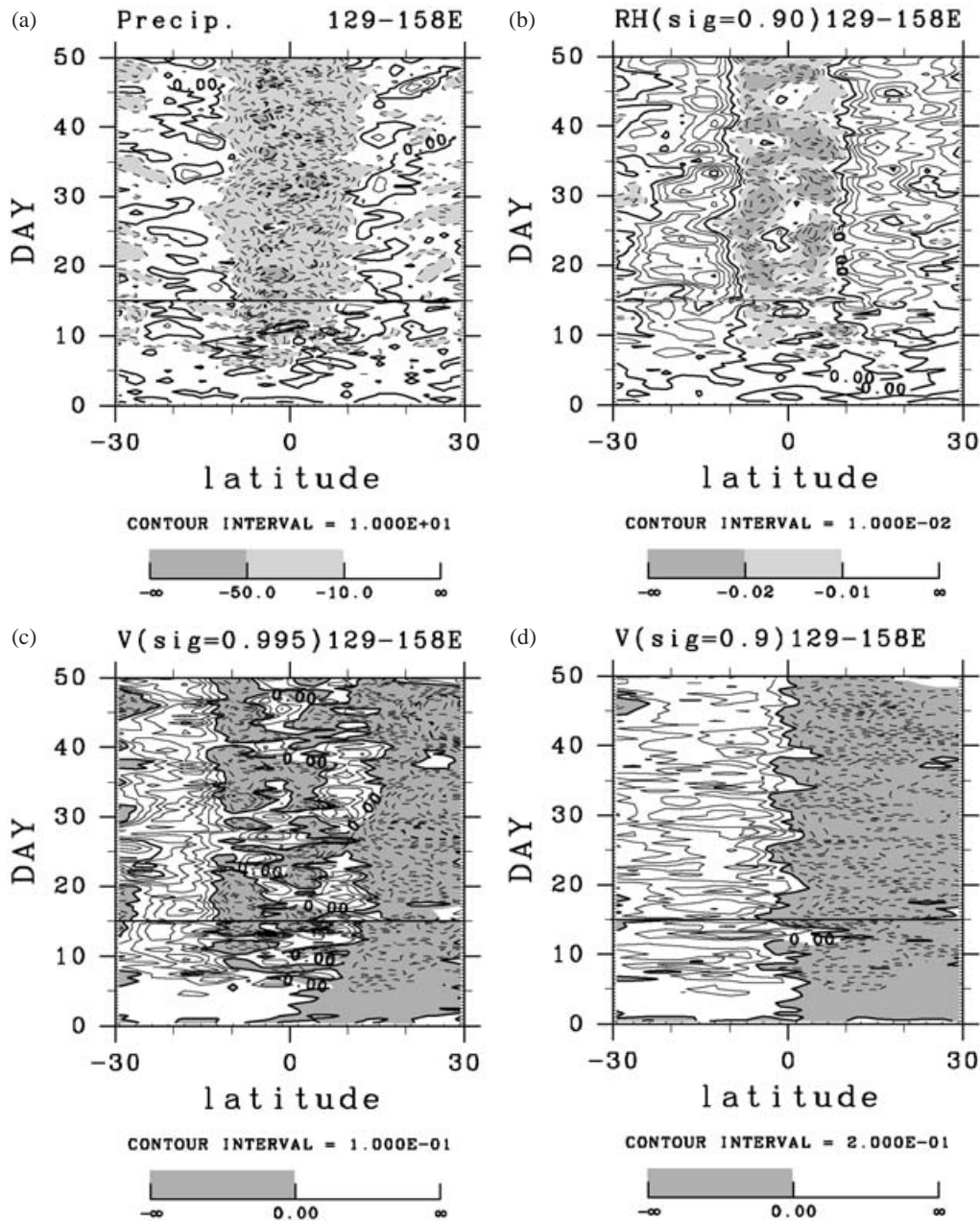


Fig. 10. Same as Fig. 9 but for the ensemble mean anomalies to the west of the warm SST area during the 50 days averaged zonally in the longitudinal region from 129° to 158° during all of 50 day integration period. Until $t = 15$ day, the ensemble mean anomaly from individual is plotted, and the ensemble mean anomaly from zonal and temporal average is plotted afterwards.

acceleration (Fig. 8 (c) and Fig. 8 (d)), suggest that the zonally symmetric pressure rise is caused rather by momentum forcing than by thermal forcing.

Figure 11 shows the development of the zon-

ally symmetric responses of zonal wind. In the very early stage (Fig. 11 (a)), zonal wind anomaly appears in the off-equatorial areas; it is westerly in the upper troposphere, while easterly in the lower troposphere. This structure

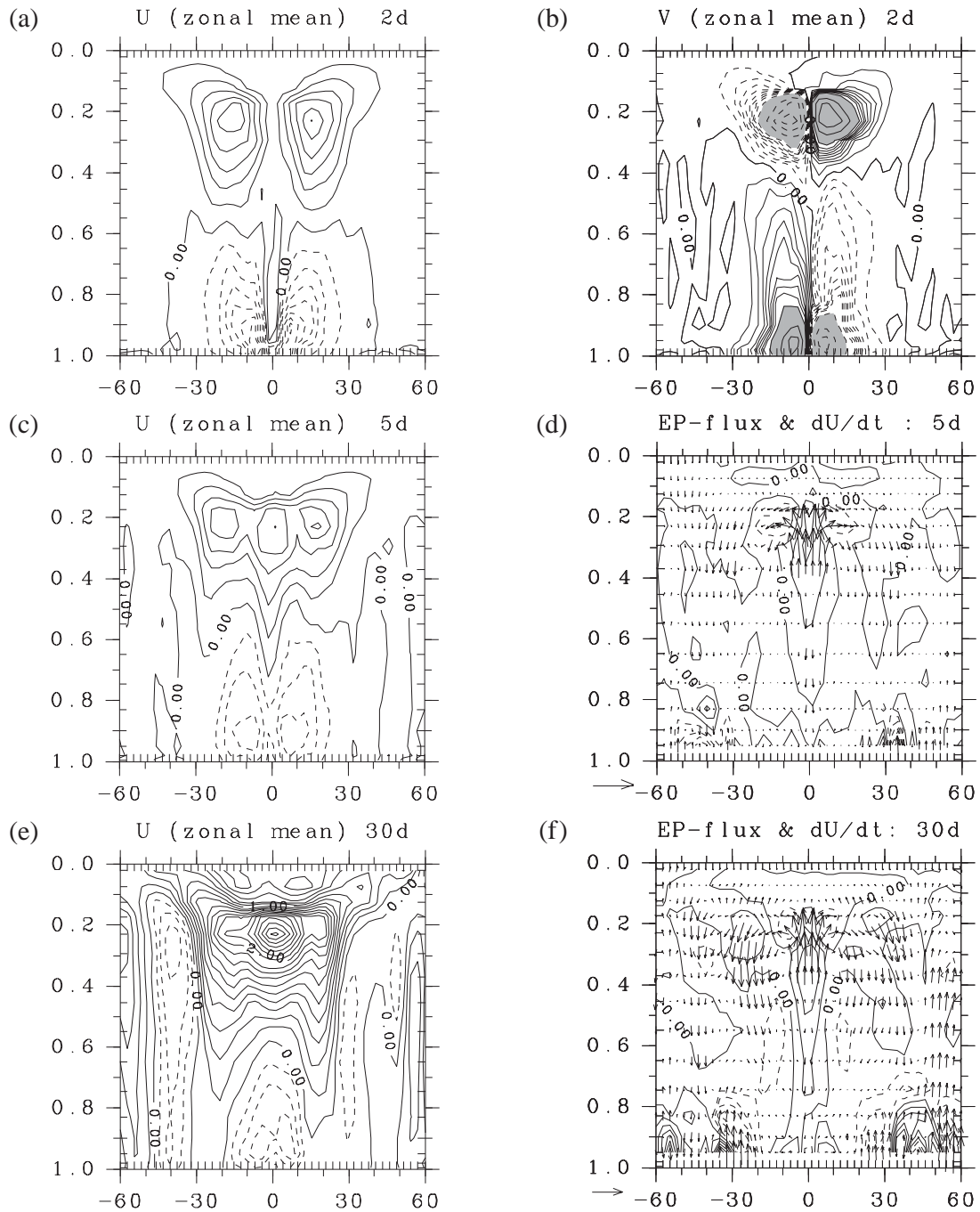


Fig. 11. Meridional sections of zonally averaged ensemble mean anomalies from individual: (a) Westerly wind at $t = 2$ day. Contour interval is 0.02 m s^{-1} . (b) Temporal average of southerly wind (v) between $t = 0$ day and $t = 4$ day. Contour intervals are 0.005 m s^{-1} and 0.05 m s^{-1} for $|v| < 0.05 \text{ m s}^{-1}$ and $|v| > 0.05 \text{ m s}^{-1}$, respectively. Regions with $|v| > 0.05 \text{ m s}^{-1}$ are shaded. (c) Westerly wind at $t = 5$ day. Contour interval is 0.1 m s^{-1} . (d) Temporal average of wave activity between $t = 2$ day and $t = 8$ day. Arrows represent Eliassen-Palm flux, and contours indicate its divergence. Length of the reference vector shown to the lower left corner corresponds to $10^{-6} \text{ m}^2 \text{ s}^{-2}$. Contour interval is 10^{-6} m s^{-2} . (e) Westerly wind at $t = 30$ day. Contour interval is 0.2 m s^{-1} . (f) Same as (d) but for the temporal average between $t = 20$ day and $t = 30$ day.

can be understood as a result of absolute angular momentum transport by the meridional circulation anomaly (Fig. 11 (b)), caused by the anomalous heating at the convection center.

At day 5 (Fig. 11 (c)), westerly anomaly appears in the equatorial middle and upper troposphere. The westerly acceleration at the equator results from the wave activity induced by the SST anomaly. Figure 11 (d) shows the ensemble mean anomaly of Eliassen-Palm flux (EP-flux) and its divergence. At the equator, the middle and upper troposphere is dominated by divergence of EP-flux anomaly. Its magnitude reaches, measured by the unit of zonal flow acceleration, 0.2 m s^{-1} per day. Major contribution to the divergence of EP-flux comes from its upward component at the equator and its off-equatorward component at around the tropopause near the equator. Namely, easterly momentum is transported upward by the negative correlation between eddy zonal flow and eddy updraft at the equator, and then, pumped out off-equatorward by the negative correlation between eddy zonal and meridional flows. The poleward EP-fluxes at around the tropopause converges at around $\pm 15^\circ$. Easterly accelerations at those areas seems to be overwhelmed by the transport of westerly wind anomaly from the equator by the Hadley circulation. Consequently, there appear areas of westerly minima at around $\pm 10^\circ$ in Fig. 11 (c).

At day 30 (Fig. 11 (e)), the regions of westerly anomaly extends downward around the latitudes of around $\pm 20^\circ$. In the poleward latitudes to these, there appear areas of easterly anomaly. In the upper troposphere, EP-flux (Fig. 11 (f)) is directed poleward and downward from the upper troposphere of the subtropics to the mid-latitudes. Correspondingly, there appear divergence of EP-flux at around $\pm 20^\circ$ and convergence at around $\pm 40^\circ$. Easterly momentum is pumped out from the tropics to the mid-latitudes by eddy activities. The downward extension of the westerly anomaly around $\pm 20^\circ$ results presumably from the downward transport of the anomalous westerly wind by the Hadley cell. These latitudes are the positions of the downward branch of the Hadley circulation as inferred from Fig. 2 (c). Figure 2 (c) shows the meridional circulation of the case without SST anomaly, but basic characters of the Hadley cell remains unchanged in the runs with

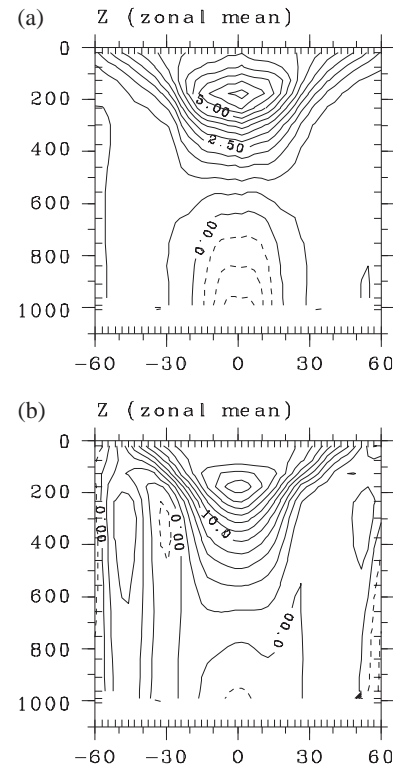


Fig. 12. (a) Meridional sections of zonally averaged ensemble mean geopotential anomaly from individual at $t = 2$ day (contour interval is 0.5 m s^{-1}). Ordinate is pressure (hPa). (b) Same as (a) but for $t = 30$ day (contour interval is 2 m s^{-1}).

SST anomaly.

The ensemble average response of zonal mean geopotential exhibits the structure of the so-called first baroclinic mode in the early stage (Fig. 12 (a)). The low level pressure anomaly is negative there. In the later stage (Fig. 12 (b)), as the low level zonal flow anomaly becomes westerly, the low level zonal mean geopotential anomaly rebounds. This can be understood as the geostrophic adjustment to the acceleration of westerly wind. The low level westerly acceleration and the positive tendency of low level geopotential continue at day 30 and after (not shown here).

The partitioning of the wave activity into the transient and the stationary components is of interest. Figure 13 shows the EP flux and its divergence calculated from the temporal mean

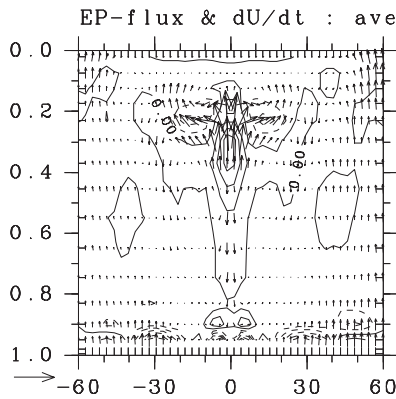


Fig. 13. Same as Fig. 11 (f) but for calculated from the temporal average of the ensemble mean response between $t = 20$ day and $t = 40$ day.

of the ensemble average response from 20 days to 40 days after the switch on of the warm SST anomaly. Comparison between Fig. 11 (f) and Fig. 13 shows that stationary waves mainly contributes to the EP-flux divergence in the equatorial upper troposphere. On the other hand, the EP-flux divergence in the subtropical upper troposphere in Fig. 11 (f) is absent in Fig. 13; the EP-flux vectors, directed poleward and downward from the upper troposphere of the subtropics to the mid-latitudes in Fig. 11 (f), result from transient waves. In short, both stationary and transient waves seem to contribute to the tropical westerly acceleration, but in different locations.

In summary, the zonally symmetric slow pressure rise seems to occur as the result of geostrophic adjustment to the low level westerly acceleration caused by the transport of angular momentum from the middle and upper equatorial troposphere, where the anomaly of wave activity accelerates the westerly wind. Unfortunately, owing to the strong noises which still remain even after the ensemble averaging, temporal averaging is indispensable to obtain a fairly smooth picture shown in Fig. 11. Even after these smoothing procedures, the obtained fields are still quite noisy in the mid- and higher latitudes; there remain not a small amount of north-south asymmetries in Fig. 11. Time evolution of wave activity is, of course, interesting, but such analyses of wave activities

is possible only with an ensemble experiment with much larger number of members.

7. Discussions and conclusions

An ensemble experiment is conducted with an aqua-planet GCM for the purpose of examining the initial development of the atmospheric response to the introduction of a warm SST anomaly. The ensemble experiment of the size of 128 is successful in extracting the initial transient atmospheric response relevant to the introduction of the warm SST anomaly, which, in a result of a single run, is buried in the transient noise due to small scale convective activity and large scale variability of the intra-seasonal time scale.

The major characteristics of the initial development of the response can be summarized as follows. In less than 1 day after the switch-on, a low pressure area emerges over the warm SST area. In a few days, the appearance of the convection center, i.e., the increase of precipitation over the SST anomaly, follows. Immediately after the appearance of the low pressure at the warm SST area, a globally distributed, barotropic, positive pressure anomaly emerges. The amplitude of the global positive anomaly is rather small, but accounts for about a half of the equatorial pressure rise observed to the west of the warm SST area in the long time mean field. At the same time, the low pressure area above the convection center begins to extend eastward as a warm moist Kelvin wave and westward as a warm moist Rossby wave. At the moist Kelvin wave front, precipitation is suppressed for a few days, but after that, precipitation rebound occurs and precipitation anomaly becomes positive. The enhancement of precipitation results from the frictional convergence in the mixed layer in the warm Kelvin wave signal. At the moist Rossby wave front, on the other hand, precipitation decreases monotonically. This is related to the divergent surface frictional wind in the mixed layer of the equatorial latitudes in the warm Rossby wave signal. Finally, there appears a zonally symmetric response within the Hadley cell, characterized with surface pressure rise in the tropics, and westerly anomaly in the upper troposphere. The westerly anomaly is created by the zonal momentum transport by the thermally forced stationary wave at the equator and the change

of transient wave activity in the subtropical upper troposphere. The westerly anomaly is transported to the lower level by the Hadley circulation, and the geostrophic adjustment to the resulting low level westerly acceleration seems to be responsible for the surface pressure rise. The tropical zonally symmetric response continues to evolve slowly and the associated equatorial pressure anomaly increases toward the value obtained in the long time mean field.

The evolution of the response captured by the ensemble experiment agrees with the following portions of the expectation of H98: the east-west asymmetry of the precipitation anomaly is caused by the surface frictional divergence at the equator which is negative (positive) in the Kelvin (Rossby) wave signal emitted to the east (west) of the convection center. On the other hand, contrary to the speculation by H98, the high pressure anomaly to the west of the warm SST area does not result from the precipitation decrease to the west of the convection center. Instead, about a half of the pressure rise develops immediately after the switch-on of the SST anomaly, as a part of global barotropic response to the heating in the convection center, and another half is associated with the slow zonally symmetric pressure rise in the tropics caused by mass redistribution between the tropics and the extratropics. The significance of these two responses in the tropical pressure field is one of the important findings of this study.

Another point of importance, which is also a success of ensemble average method, is that the propagation of moist Kelvin wave is clearly identified and that the propagation of the major part of the response occurs in the form of moist Kelvin wave. The noteworthy point is that information on the occurrence of some change extending the full depth of the troposphere at the equator tends to propagate eastward, not at the speed of a dry Kelvin wave, but at the speed of a moist Kelvin wave. The eastern front of the response propagates quite coherently at the speed of about 18 m s^{-1} , which is significantly slower than the phase speed of dry Kelvin wave of the same vertical structure (about 40 m s^{-1}). This slow propagation is explained by the positive correlation between the heating and vertical velocity at the warm Kelvin wave front in the ensemble response. We have to confess, however, that quantitative analyses of the

nature of moist Kelvin wave could not be performed in the present study. More quantitative analysis is required to describe the amount of reduction of stability and phase speed by moist processes in the model.

The Rossby wave front to the west is rather blurred compared to the Kelvin wave front to the east. An explanation of this difference can be proposed from the dispersion relation of equatorial waves; Rossby wave is dispersive, while Kelvin wave is non-dispersive. In particular, at the zonal wavelength comparable to, or shorter than the radius of deformation, Rossby wave is strongly dispersive. According to the latitudes of trough associated with Rossby response in our results, the "moist" radius of deformation can be roughly estimated as around 1000 km. This means that the Rossby wave front should be strongly dispersive. In order to describe the behavior of westward propagating moist Rossby wave front, equatorial wave theory with long-wave approximation (e.g., Gill 1980) is inadequate.

Hoskins et al. (1999) reported an aqua-planet GCM experiment with a localized SST anomaly over the equator with different set-ups (such as the distribution of SST, the discretization of basic equations, and, cumulus parameterization) from H98. They also obtained westerly acceleration in the upper troposphere at the equator, but its magnitude is much larger than that in the present study. Although quantitative analysis of the aqua-planet GCM is not presented, they propose the angular momentum transport by the Hadley cell and the wave activity, namely the $u'v'$ term, as possible causes of the super rotation, referring the results of experiments using a simple model. In contrast to their speculation, the present result indicates $u'w'$ term is important at the equator.

It should also be noted that the precipitation response outside the warm SST anomaly in Hoskins et al. (1999) differs significantly from ours. Most importantly, the rainfall decreases both to the west and to the east of the SST anomaly in their experiment. Presently, we have no particular idea for the discrepancy between their response and ours, because a number of differences exist between their setup and ours. One of the important examples is the lack of clouds and their interaction with the short and long wave radiative forcing in our GCM,

which may affect not only the structure of the stationary responses, but also the behavior of the transient responses, e.g., the propagation speed of the moist Kelvin wave. In order to resolve this issue, comparison of aqua-planet experiments with different GCM, as is proposed by Neale and Hoskins (2000a,b), may be helpful.

The present study have at least two implications concerning the real atmosphere. The first point is that the time scale of the adjustment of the precipitation anomaly, about 15 days, is not negligible compared to the time scale of seasonal variability of the SST or the onset time of ENSO. The response time cannot be neglected when one considers the response of convection to the evolution of SST in real atmospheric conditions. This implies, for example, that a simplified coupled atmosphere-ocean model should include a certain finite lag representing the development of precipitation anomaly forced by the SST signature. Matthews (2000) already pointed out the significance of this lag or the "adjustment process" regarding the eastward propagation of intraseasonal variability in the real atmosphere, but its potential role in the air-sea interaction process remains unclear.

Second point is the significance of the globally distributed rapid barotropic response. The existence of the signal associated with barotropic modes in the real atmosphere has been reported, for example, by Hamilton and Garcia (1986) or Matthews and Madden (2000). They reported that the activity of Kelvin waves that have the frequency of 33 hours is modulated by the activity of seasonal and interannual variabilities. Unfortunately, suffering from low temporal resolution of OLR data, they could not find any positive evidence on the further relationship between activities of the barotropic Kelvin wave and deep convection. The present study strongly suggests that those waves can be excited by the variation of precipitation. It must be interesting to examine the relationship between precipitation and global pressure variation, using observational data or results of more realistic GCM experiments.

Acknowledgements

The numerical integrations were performed at the supercomputer (NEC SX-4) of the Center

for Global Environmental Research, National Institute for Environmental Studies (<http://www.nies.go.jp/>). The software and local computational and information environments were constructed by the use of the resources of GFD-DENNOU CLUB (<http://www.gfd-dennou.org/>). The authors thank Takeshi Horinouti at the Research Institute for Sustainable Humansphere of Kyoto University for providing tools for EP-flux calculation. A number of valuable comments by the anonymous reviewers are greatly helpful in improving the manuscript.

Reference

- Gill, A.E., 1980: Some simple solutions for heat-induced tropical circulation. *Quart. J. Roy. Meteor. Soc.*, **106**, 447–462.
- , 1982a: Section 6.17, *Atmosphere-ocean dynamics*, Academic Press., New York. 662pp.
- , 1982b: Studies of moisture effects in simple atmospheric models: the stable case. *Geophys. Astrophys. Fluid Dynamics*, **19**, 119–152.
- Hamilton, K., and R.R. Garcia, 1986: Theory and observations of the Short-period normal mode oscillations of the atmosphere. *J. Geophys. Res.*, **91**, 11867–11875.
- Hayashi, Y.-Y., E. Toyoda, M. Hosaka, S. Takehiro, K. Nakajima, and M. Ishiwatari, 2000: Tropical precipitation patterns in response to a local warm SST area placed at the equator of an aqua planet. *CGER's supercomputer monograph report*, **6**.
- Heckley, W.A., and A.E. Gill, 1984: Some simple analytical solutions to the problems of forced equatorial long waves. *Quart. J. Roy. Meteor. Soc.*, **110**, 203–217.
- Hosaka, M., M. Ishiwatari, S. Takehiro, K. Nakajima, and Y.-Y. Hayashi, 1998: Tropical precipitation patterns in response to a local warm SST area placed at the equator of an aqua planet. *J. Meteor. Soc. Japan*, **76**, 289–305.
- Hoskins, B.J., R. Neale, M. Rodwell, and G.-Y. Yang, 1999: Aspects of the large-scale tropical atmospheric circulation. *Tellus*, **51A–B**, 33–44.
- Kasahara, A., and Y. Shigehisa, 1983: Orthogonal vertical normal modes of a vertically staggered discretized atmospheric model. *Mon. Wea. Rev.*, **111**, 1724–1735.
- Louis, J.-F., 1979: A parametric model of vertical eddy fluxes in the atmosphere, *Bound. Layer Meteor.*, **17**, 187–202.
- Madden, R.A., and P.R. Julian, 1972: Description of global-scale circulation cells in the tropics with a 40–50 day period. *J. Atmos. Sci.*, **29**, 1109–1123.

- Manabe, S., J. Smagorinsky, and R.F. Strickler, 1965: Simulated climatology of a general circulation model with a hydrologic cycle. *Mon. Wea. Rev.*, **93**, 769–798.
- Matsuno, T., 1966: Quasi-geostrophic motions in the equatorial area. *J. Meteor. Soc. Japan*, **44**, 25–43.
- Matthews, A.J., 2000: Propagation mechanisms for the Madden-Julian Oscillation. *Quart. J. Roy. Meteor. Soc.*, **126**, 2637–2651.
- , and R.A. Madden, 2000: Observed propagation and structure of the 33-h atmospheric Kelvin wave. *J. Atmos. Sci.*, **57**, 3488–3497.
- Mellor, G.L., and T. Yamada, 1974: A hierarchy of turbulence closure models for the planetary boundary layers. *J. Atmos. Sci.*, **31**, 1791–1806.
- Neale, R.B., and Hoskins, B.J., 2000a: A standard test for AGCMs including their physical parameterizations: I: The proposal. *Atmos. Sci. Lett.*, **1**, 101–107.
- , and ———, 2000b: A standard test for AGCMs including their physical parameterizations. II: Results for the Met Office model. *Atmos. Sci. Lett.*, **1**, 108–114.
- Nicholls, M.E., and R.A. Pielke, 1994: Thermal compression waves. I: Total-energy transfer. *Quart. J. Roy. Meteor. Soc.*, **120**, 305–332.
- Numaguti, A., 1992: Numerical experiments on the large scale structure of cumulus activity in the tropics. Ph.D. Thesis, University of Tokyo. (in Japanese). 205pp.
- , and Y.-Y. Hayashi, 1991: Behavior of cumulus activity and the structure of circulations in an aqua planet model. 1. The structure of the super clusters., *J. Meteor. Soc. Japan*, **69**, 541–561.
- Swamp Project, 1998: AGCM5. <http://www.gfd-dennou.org/arch/agcm5/>, GFD Dennou Club.
- Toyoda, E., K. Nakajima, M. Ishiwatari, and Y.-Y. Hayashi, 1999: Response of the tropical atmosphere to a localized warm SST area: Time-development observed in an aqua-planet ensemble experiment. *Nagare*, **18**, <http://www.nagare.or.jp/mm/99/toyoda/>.